Dhaka Univ. J. Sci. 74(1): 17-26, 2026 (January)
Prof. M. Muhibur Rahman Memorial Issue
ISSN 1022 - 2502, E-ISSN 2408- 8528
DOI: https://doi.org/10.3329/dujs.v74i1.84725

Adsorptive Detoxification of m-Cresol from Wastewater using Nano La_2NiMnO_6 Double Perovskites

Syed Abdul Monim[1,2], Shawon Saha[1], Md. Minhajul Alam Khan[1], Iqbal Mahmud[2], and Shakhawat H. Firoz[1]*

[1]*Department of Chemistry, Bangladesh University of Engineering and Technology (BUET), Dhaka-1000, Bangladesh*
[2] *Eastern University, Dhaka, Bangladesh*

(Received : 30 September 2025; Accepted : 23 December 2025)

Abstract

A simple sol-gel method was developed to synthesize La_2NiMnO_6 (LNMO) double perovskite in nano dimensions, which was evaluated for the effective adsorptive removal of m-cresol from aqueous solutions. The structural and chemical properties of the synthesized LNMO were characterized using X-ray Diffraction (XRD), Fourier transform infrared (FTIR) spectroscopy, Field Emission Scanning Electron Microscopy (FESEM), and Inductively Coupled Plasma Optical Emission Spectroscopy (ICP-OES). The LNMO material possessed a hexagonal crystal structure and an average particle size of approximately 50 nm, which contributed to improving adsorptive properties. Furthermore, adsorption studies revealed that m-Cresol removal is significantly pH dependent, as maximum adsorption was found at pH 2. As a weak acid, m-cresol exists in its neutral form in acidic conditions and promotes interaction through hydrogen bonding and Lewis acid-base interactions with LNMO's surface. Moreover, adsorption isotherms were analyzed using Langmuir, Freundlich, and Temkin model where the Langmuir model fitted the best, indicating a maximum adsorption capacity of 204 mg/g while the values of Langmuir equilibrium constant (K_L) of 0.1158 L/mg, and a dimensionless constant (R_L) of 0.256, suggesting a favorable adsorption process. Thermodynamic parameters like Gibbs free energy (ΔG^o), enthalpy (ΔH^o), and entropy change (ΔS^o) were analyzed, and it revealed that the adsorption process is spontaneous, heat-releasing, and leads to reduced randomness at the solid-liquid interface. Hence, this study demonstrates the exceptional potential of LNMO as an efficient, cost-effective adsorbent for m-cresol removal, offering valuable insights for the development of novel material for wastewater treatment.

Keywords: Double perovskite, m-cresol, detoxification, adsorbent, optimization, adsorption capacity

I. Introduction

m-cresol is a phenolic compound that is extensively used in pharmaceuticals, petrochemicals, agrochemicals, and oil refining industries[1-3]. Its acute toxicity and non-biodegradable nature pose a threat to humans and the aquatic ecosystem when disposed of untreated into the environment[4]. The International Maritime Organization (IMO) ranked m-cresol as one of the top twenty hazardous and noxious substances[5]. Due to its high-water solubility, m-cresol is frequently detected in industrial effluents at concentrations ranging from 21.5 to 26.0 g L^{-1}[6]. Consequently, the development of effective removal of m-cresol from wastewater is essential to prevent environmental contamination.

Over the past few decades, various physicochemical and biological methods have been employed for the removal of phenolic compounds, including oxidation, coagulation, precipitation, adsorption, biological treatments, and membrane filtration[7,8]. Previous works suggest that adsorption-based decontamination is the most effective process due to its energy efficiency and environmental compatibility[9]. A wide range of adsorbents has been explored, including carbonaceous materials, polymers, metal oxides, hydrogels, and more recently, perovskite-based materials[10]. It is worth mentioning that, in recent years, perovskite-based materials have emerged as promising adsorbents, owing to their unique crystal structure and rich redox chemistry, which facilitate multiple interaction pathways during adsorption, including electrostatic attraction, cation–π interactions, etc.[11].

Perovskites are ceramic mixed oxides with the general formula ABO_3, where A is typically an alkaline earth or rare-earth metal, and B is a transition metal[12]. Their unique crystal structure, high stability, mixed oxidation states, and abundant oxygen vacancies provide multiple active sites for pollutant binding, making them promising candidates for adsorption applications. Several studies have reported their potential in wastewater remediation[13,14]. For instance, Deng et al.[15] demonstrated the efficient adsorption of Rhodamine B (RhB) on $LaFeO_3$ through a combination of electrostatic interactions, hydrogen bonding, Lewis acid-base interaction, and cation–π interactions between the dye and the adsorbent. In another study, Shahheydar et al.[16] demonstrated the high adsorption capacity and recyclability of $La_{0.8}Ca_{0.2}MnO_3$ nanoparticles for the removal of Eriochrome Cyanine R dye. Recently, a new class of double perovskites ($A_2BB'O_6$) has gained attention as an advanced functional material. Unlike single ABO_3 perovskites, double perovskites exhibit cooperative redox chemistry and paired surface sites that enhance their reactivity[17,18]. Double perovskites exhibit defect-tolerant structures, tunable acid–base properties, and oxygen vacancy-driven surface chemistry, making them attractive candidates as an adsorbent for environmental remediation[19]. In current reported studies, Lanthanum-based double

*Author for correspondence. e-mail: shfiroz@chem.buet.ac.bd

perovskites such as La_2NiMnO_6, La_2FeMnO_6, and La_2FeCrO_6 have been investigated for applications in energy storage, solar cells, electro-catalysis, and optoelectronics[20,21]. It is noteworthy that, beyond their energy-related applications, La-based perovskites have also been investigated as efficient adsorbents. For example, CTAB-capped $La_{0.9}Sr_{0.1}FeO_3$ perovskite exhibited a remarkable adsorption capacity of 151.52 mg/g^{-1} for Rhodamine RhB removal[22]. However, most of the reported studies to date have focused on single perovskite systems, whereas the application of double perovskites for the adsorptive removal of organic pollutants remains largely underexplored, despite their promising structural versatility and tunable surface chemistry. In this context, La_2NiMnO_6 (LNMO) can be considered as a promising candidate for adsorptive removal of organic pollutants like m-cresol. It can be anticipated that the mixed oxidation states of Ni and Mn can promote Lewis acid–base interactions with the phenolic oxygen of m-cresol, while the oxygen vacancies can facilitate π–π interactions with its aromatic ring[14,23-26]. These intrinsic properties make LNMO a promising candidate for efficient adsorptive removal of phenolic contaminants[14,24,25].

In this study, LNMO double perovskite was synthesized via the sol-gel method and subsequently characterized using a range of analytical techniques. Its adsorption performance for removing m-cresol from aqueous solutions was thoroughly examined. Particular emphasis was placed on assessing adsorption efficiency under different operational conditions, such as pH, contact time, initial concentration, and temperature, to bridge the existing research gap in utilizing double perovskite oxides as innovative adsorbents for m-cresol removal from wastewater.

II. Materials and Methods

Materials

Lanthanum (III) Nitrate Hexahydrate ($La(NO_3)_3.6H_2O$; Acros Organics, France), Nickel (II) Nitrate Hexahydrate ($Ni(NO_3)_2.6H_2O$; Alpha Chemika, India), Manganese (II) Acetate Tetrahydrate ($Mn(C_2H_3O_2)_2.4H_2O$; Alfa Aesar, UK), Citric acid monohydrate ($(C_6H_8O_7).H_2O$; Acros Organics, France), m-Cresol (C_7H_8O; Loba Chemie, India), Sodium hydroxide powder (NaOH; Sigma Aldrich, USA), Hydrochloric Acid (HCl; Pursuit Industries, India) were purchased. All chemicals used were of analytical grade and applied directly without additional purification. Solutions required for the experiments were prepared using deionized (DI) water (2 µs cm^{-1}). The DI water was sourced from a Barnstead nano-pure water purification system (Thermo Scientific, USA).

Preparation and characterization of LNMO

LNMO double perovskites were synthesized using a sol-gel method. The required stoichiometric ratios of nitrate salts of La, Ni, and acetate salts of Mn were mixed in water for injection (WFI), followed by the addition of citric acid, and the mixture was stirred at room temperature for an hour. Subsequently, the solution was heated at 70 °C while shaking to form a gel. The excess water was removed by drying the gel at 130 °C for 10 hours, followed by annealing at 800 °C for 6 hours in air to obtain the final product.

Characterization

The structural and crystallographic characterization of the synthesized products was conducted via X-ray Diffraction (XRD) using a Rigaku Ultima IV diffractometer (Rikagu corporation, Tokyo, Japan) and chemical functional groups were analyzed using Fourier Transform Infrared spectroscopy (FTIR) using an FTIR-8400 instrument (Shimadzu, Japan). The surface morphology was further analyzed via a Field-Emission Scanning Electron Microscopy (FESEM) (JEOL Ltd, Tokyo, Japan), and compositional analysis was performed via Inductively Coupled Plasma Optical Emission Spectroscopy (ICP-OES).

Adsorption Test

The adsorption performance of the synthesized LNMO double perovskite was systematically examined under varying experimental conditions, including solution pH, initial m-cresol concentration, temperature, and contact time, to optimize the adsorption process. A fixed adsorbent dosage of 50 mg (0.5 g L^{-1}) was used in all experiments. Batch adsorption studies were carried out in 250 mL conical flasks containing 100 mL of m-cresol solution with an initial concentration of 50 ppm. The pH of the solution was adjusted in the range of 2 to 10, while the effects of concentration, temperature, and contact time were independently investigated. Following each adsorption cycle, the residual concentration of m-cresol was determined by measuring absorbance at 275 nm using a UV–Vis spectrophotometer, thereby evaluating the adsorption efficiency of LNMO. Moreover, the removal and adsorption capacity of LNMO towards m-cresol were calculated using the following equations, eq^n 1 and eq^n 2[27,28],

$$\%\, removal\ (\%R) = \left(\frac{(C_i - C_e)V}{C_i}\right) \times 100\% \ldots\ldots\ldots\ldots\ldots\ (1)$$

$$Adsorption\ Capacity\ (Q_e) = \frac{(C_i - C_e)V}{m} \ldots\ldots\ldots\ldots\ldots\ (2)$$

Where Ci and Ce are the influent and effluent concentration of m-cresol (mg/L), V (L) is the volume of m-Cresol, and m (g) is the amount of adsorbent used.

Isotherm analysis

The adsorption isotherm was evaluated using three different isotherm models: Langmuir, Freundlich, and Temkin. The linearized forms of the Langmuir, Freundlich, and Temkin isotherm equations are presented below[27].

$$\frac{C_e}{Q_e} = \frac{1}{Q_m K_L} + \frac{C_e}{Q_m} \ldots\ldots\ldots\ldots\ldots\ldots\ (3)$$

$$lnQ_e = lnK_F + \frac{1}{n} lnC_e \ldots\ldots\ldots\ldots\ldots\ldots\ (4)$$

$$Q_e = b_T ln K_T + b_T ln C_e \ldots\ldots\ldots\ldots\ldots\ldots\ldots\ldots (5)$$

In the Langmuir isotherm, K_L (L/mg) is the Langmuir equilibrium constant. The Freundlich isotherm uses K_F (mg/g) as its constant, while n is the adsorption intensity parameter. For the Temkin model, K_T (L/g) represents the equilibrium binding constant, and b_T (KJ/mol) is the Temkin constant. The parameter Q_m (mg/g) indicates the theoretical adsorption capacity, whereas Q_e (mg/g) is the experimentally observed adsorption capacity, and C_e is the equilibrium concentration.

Kinetic analysis

The adsorption kinetics were investigated over a time interval ranging from 0 to 90 minutes. The experiments were conducted using a 50-ppm solution with an adsorbent dosage of 50 mg at pH 2. The kinetic results were analyzed using pseudo-first-order and pseudo-second-order models. The linearized forms of these models are provided in the following equations[28].

$$ln(Q_e - Q_t) = ln Q_e - k_t t \ldots\ldots\ldots\ldots\ldots (6)$$

$$\frac{t}{Q_t} = \frac{1}{k_2 {Q_e}^2} + \frac{1}{Q_e} \ldots\ldots\ldots\ldots\ldots\ldots\ldots\ldots\ldots (7)$$

In these kinetic models, Q_e (mg/g) is the equilibrium adsorption capacity, while Q_t (mg/g) is the amount adsorbed at a specific time t (min). The parameter k_1 (min^{-1}) is the rate constant of the pseudo-first-order model, and k_2 ($g \cdot mg^{-1} \cdot min^{-1}$) corresponds to the rate constant of the pseudo-second-order model.

Thermodynamic study

The thermodynamic behavior of the adsorption process was investigated at different temperatures (25, 40, 60, and 80 °C). The thermodynamic parameters, including ΔG°, ΔH°, and ΔS°, were determined from the temperature-dependent variation of the K_L using the appropriate thermodynamic equation[29].

$$\Delta G^o = -RT ln K_L \ldots\ldots\ldots\ldots\ldots\ldots (8)$$

$$\Delta G^o = \Delta H^o - T\Delta S^o \ldots\ldots\ldots\ldots\ldots (9)$$

$$ln K_L = -\frac{\Delta H^o}{RT} + \frac{\Delta S^o}{R} \ldots\ldots\ldots\ldots\ldots (10)$$

Where, K_L is the equilibrium constant obtained from the Langmuir equation ($K_L = Q_e/C_e$ calculated in different temperatures 298 K, 313 K, 333 K, 353 K), ΔH^o is the enthalpy, ΔS^o is the entropy, ΔG^o is the Gibbs free energy, R is the universal gas constant (8.314 J $mol^{-1}K^{-1}$), and T is the temperature of the system temperature.

III. Results and Discussion

Characterization

The crystalline structure and phase purity of LNMO were analyzed by XRD patterns, which are depicted in Fig. 1(a). It's worth mentioning that during calcination, the gel precursor undergoes thermal decomposition that facilitates the removal of volatile species and organic residues, leading to the formation of a well-ordered crystal structure as shown in Fig. 1(a). This high-temperature process facilitates the rearrangement of atoms, leading to the formation of a stable and well-ordered crystal lattice. Moreover, the XRD diffraction patterns of the synthesized material match well with the standard pattern of LNMO (ICDD: 01-075-2900), belonging to hexagonal symmetry with a space group of R-3c[30]. No secondary phase or other single or multi-oxide impurities were observed, confirming the formation of phase-pure hexagonal LNMO crystal system. To gain an in-depth insight into the crystal structure, the lattice parameters were calculated and presented in Table 1.

Table 1. Structural parameters by means of space group, lattice parameters, cell volume and crystallite size of LNMO double perovskite

Space group	Lattice parameters							Crystallite size/nm
	a / Å	b / Å	c / Å	α / deg.	β / deg.	γ / deg.	Cell volume/$Å^3$	
R-3c	5.4372	5.4394	13.1281	90	90	120	388.2649	47

Furthermore, FTIR analysis was performed to assess if distortions arise from octahedral sites at the LNMO double perovskite. In our recently published work, where LMNO was synthesized, the full spectral range, including weak or residual bands of FTIR analysis[26]. It is observed that the FTIR spectrum of the LNMO precursor intermediate in its gel form dried at 130° C consisted of a complex of citric acid, nitrates, and metal ions. After the annealing process, no peaks accompanying citrate or nitrate groups are detected in any of the spectra, suggesting the purity of the perovskites. In the present case, a similar observation was made. In the Fig. 1(b), the FTIR spectrum of LNMO reveals an intense energy peak (around 562 cm^{-1}), which indicates the anti-symmetric stretching of the octahedron $Ni(Mn)O_6$. Additionally, no peaks accompanying citrate or nitrate groups or other organic groups were observed. The FTIR spectrum exhibits a distortion in the octahedral sites of Ni and Mn, which gave rise to stretching at about 562 cm^{-1}. Such distortion in the octahedral sites significantly influences the electronic and catalytic properties of perovskite materials[31,32].

Moreover, Fig. 1(c) reveals the FESEM image of LNMO, and this shows that the particles formed are mostly oblate

ellipsoids-shaped and agglomerated. The particles are closely packed and interconnected, forming a porous and rough texture which is expected to offer a sufficient active site for adsorption. The presence of inter-particle spaces suggests that LNMO possesses accessible surface sites and channels, which are favorable for adsorbate diffusion and interaction during the adsorption process. The particle size distribution curve depicted in Fig. 1(d), shows that the mean particle size of LNMO is 50.15±9.73 nm. The mean particle size obtained from particle size distribution analysis is in close agreement with the crystallite size estimated from XRD (≈47 nm), indicating that the LNMO particles are predominantly single-crystalline, with each particle corresponding to a single coherent diffraction domain, which is favorable for properties such as structural stability and electrochemical performance.

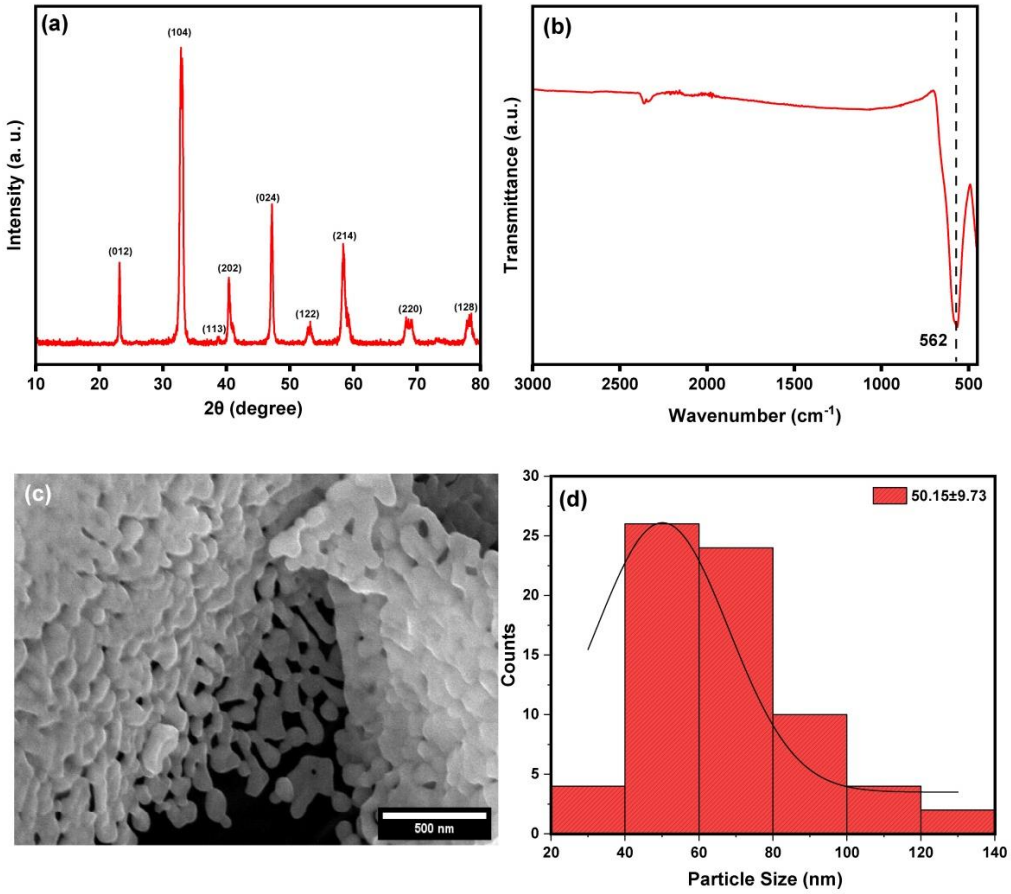

Fig. 1. Characterization of LNMO: (a) XRD patterns, (b) FT-IR spectrum, (c) FESEM and (d) Particle size distribution curve of LNMO.

Finally, the elemental composition of LNMO was measured using ICP-OES, and the results are represented in Table 2. The measured molar ratio of La:Ni:Mn is almost the same as the target concentration for achieving a molar ratio of 2:1:1. The ICP-OES measurements suggest the successful synthesis of the target double perovskite.

Table 2. The elemental concentrations in LNMO double perovskite, determined by ICP-OES

The concentrations of metal elements calculated by ICP-OES measurements				Molar ratio
Sample	La (mgL^{-1})	Ni (mgL^{-1})	Mn (mgL^{-1})	La: Ni: Mn
LNMO	14.45	3.24	2.91	1.96:1.04:1.00

Optimization of adsorption parameters

Adsorption capacity varies with changing experimental conditions such as, initial concentration of adsorbate, pH of the experiment, adsorption time, and temperature. Hence, the adsorption parameters towards m-cresol were optimized initially to devise suitable adsorption conditions. The adsorption capacity and removal efficiency of LNMO for m-cresol under different operating conditions is presented in Fig. 2.

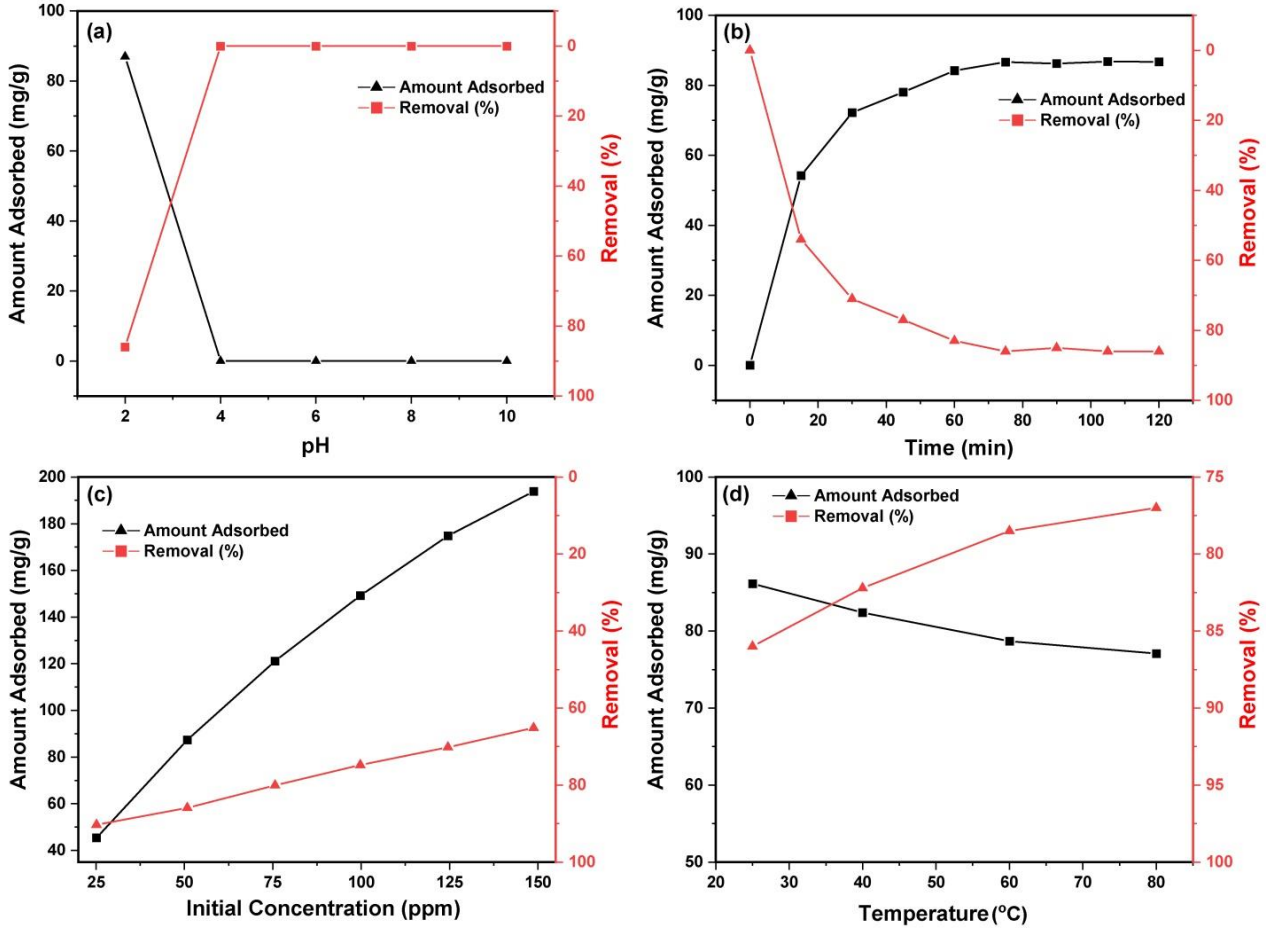

Fig. 2. Effect of different parameters on m-cresol adsorption by LNMO: (a) Effect of pH, (b) Effect of contact time, (c) Effect of initial m-cresol concentration and (d) Effect of temperature.

The effect of pH on the m-cresol adsorption is depicted in Fig. 2(a). The adsorption performance of LNMO is highly pH dependent, with maximum removal efficiency and adsorption capacity observed at pH 2; however, no further adsorption occurs as pH rises. At pH 2, the surface oxygen of LNMO becomes highly protonated and forms $M\text{-}OH_2^+$. On the other hand, at acidic pH conditions, m-cresol predominantly exists in its neutral state, whereas at higher pH or alkaline conditions, the anionic form of m-cresol predominates[33,34]. In this state, adsorption is facilitated primarily through H-bonding between the -OH of m-cresol and surface $-OH_2^+$. Additionally, Lewis acid-base interactions between the phenolic oxygen and surface Ni^{2+}/Mn^{3+} sites further promote adsorption[26]. These combined interactions account for the high adsorption capacity at pH 2. In contrast, at higher pH, m-cresol undergoes deprotonation, forming the negatively charged cresolate ion $(C_6H_4\text{-}O^-)$[33,34]. Simultaneously, the surface hydroxyl groups of LNMO also deprotonate, resulting in a negatively charged adsorbent surface. This dual deprotonation leads to strong electrostatic repulsion between the cresolate anion and the perovskite surface, significantly hindering adsorption. The schematic illustration of the adsorption mechanism of m-cresol on the LNMO surface is shown in Fig. 3.

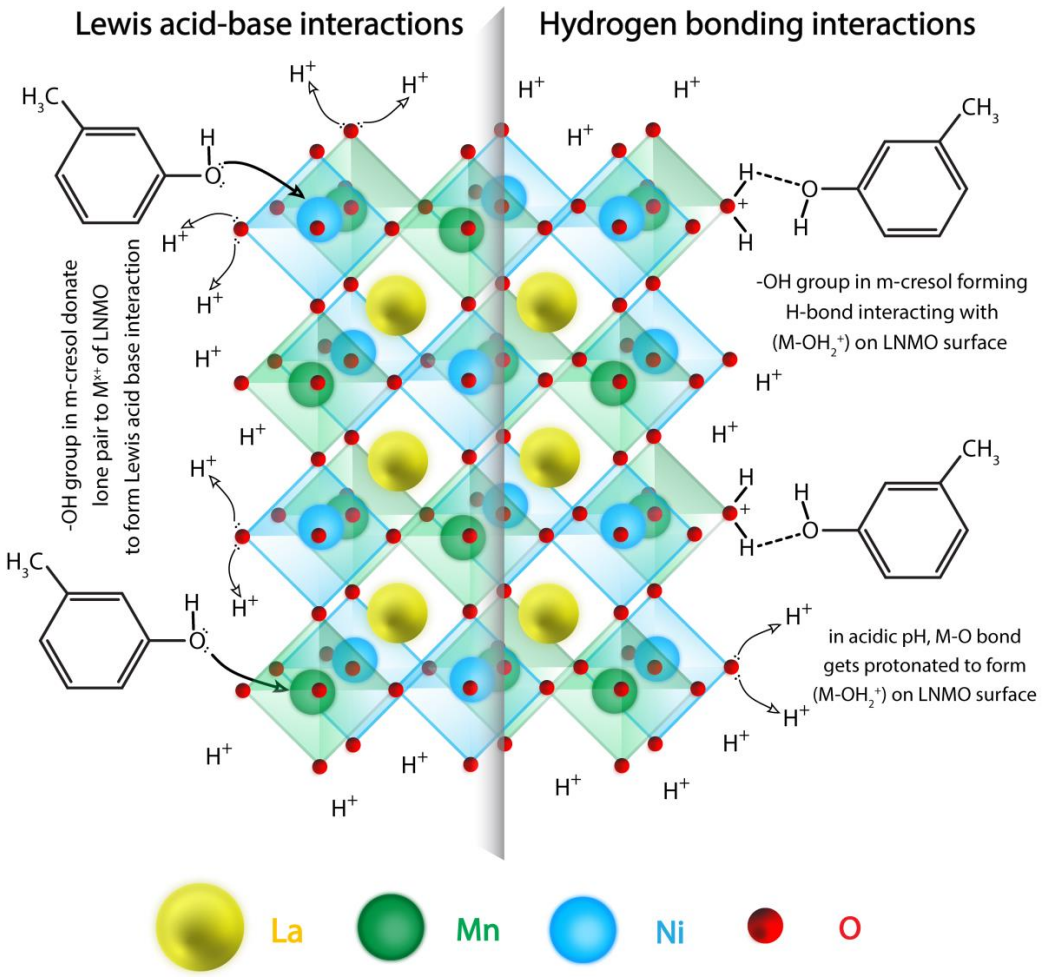

Fig. 3. Schematic illustration of the adsorption mechanism of m-cresol on the LNMO surface at acidic pH.

The effect of contact time on the removal of m-cresol was observed as shown in Fig. 2(b). It is observed that more than 50% adsorption occurred within 15 minutes, and equilibrium was reached after approximately 75 minutes, which suggests that the adsorption follows a two-stage process. At the early stage, adsorption rises steeply up to the first 45 minutes, and later, the rate decreases during 45-75 minutes, indicating that a fast external mass transfer is shadowed by a slower intra-particle diffusion, which happens to reach equilibrium. Fig. 2(c) represents the plot of adsorption capacity and removal (%) of LNMO at different m-cresol concentrations (25, 50, 75, 100, 125 and 150 ppm). Adsorption capacity increased as phenolic contaminant concentration increased, and the removal (%) decreased. Up to 50 ppm, the removal (%) is over 80%, which is satisfactory in commercial implementation. Hence, a 50ppm initial concentration of m-cresol was considered the optimized concentration of pollutant for this study. According to Fig. 2(d), the adsorption of m-cresol decreased (from 86% to 76%) with an increase in temperature from 298 K to 353 K, indicating an exothermic adsorption process. A summary of the optimum adsorption conditions for m-cresol on the LNMO surface is presented in Table 3.

Table 3. Summary of optimum adsorption conditions for m-cresol

Parameter	Optimized Condition
pH	Maximum removal efficiency and adsorption capacity were observed at pH 2
Time	50% adsorption after the first 15 minutes, and equilibrium was reached after approximately 75 minutes
Concentration	Up to 50 ppm, the removal (%) is over 80%, which is satisfactory in commercial implementation. Hence, 50 ppm of m-cresol was considered the optimum.
Temperature	The maximum 86% adsorption of m-cresol was obtained at 298 K, which was decreased (from 86% to 76%) with the increase of temperature

Adsorption Isotherms

To understand the adsorption process, the data were fitted with the Langmuir, Freundlich, and Temkin isothermal models, which are depicted in Fig. 4(a-c). Based on R^2, the equilibrium data fit the Langmuir model better than the Freundlich and Temkin models[27]. The basis of the assumptions for the Langmuir model is the specific

homogeneous surface of the adsorbent, along with monolayer adsorption. The maximum adsorption capacity, Q_{max}, determined using the Langmuir model, is 204 mg/g for the LNMO surface, as reported in Table 4.

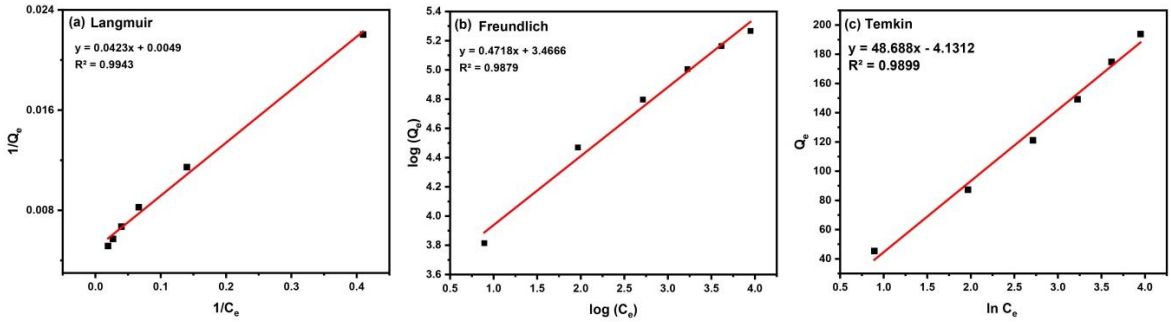

Fig. 4. Different isothermal models on the adsorption of m-cresol by LNMO: (a) Langmuir, (b) Freundlich and (c) Temkin.

The Freundlich isotherm, which indicates heterogeneous surface adsorption, also produced a moderate fit (R^2 = 0.987), with a Freundlich constant of 3.46 (mg/g^{-1}), 1/n, and a heterogeneity factor of 0.47. The value of 1/n less than 1 represents favorable adsorption and low surface heterogeneity.

Table 4. Isotherm modeling parameters obtained from the Langmuir, the Freundlich, and the Temkin models

Adsorbent	Langmuir				Freundlich				Temkin		
	Q_{max} (mg/g^{-1})	K_L	R_L	R^2	K_F	1/n	n	R^2	B_T	K_T	R^2
La_2NiMnO_6 (LNMO)	204	0.1158	0.25621	0.994	3.46	0.47	0.47	0.987	48.69	0.92	0.989

The Temkin model, which informs adsorbate–adsorbent interactions, also yielded a good agreement with the data (R^2 = 0.989), producing a Temkin binding constant of 0.92 and a heat of sorption constant of 48.69 mg/g^{-1}. These values advocate reasonable interaction energies and the existence of low heterogeneity, and the formation of a monolayer during adsorption.

Adsorption Kinetics

Furthermore, the pseudo-first and pseudo-second order kinetic models were evaluated to understand the adsorption kinetics of the LNMO[28]. From the representation of Fig. 5 and Table 5, it can be seen that the pseudo-second order model gives an excellent regression value (R^2 = 0.995) for the adsorption of m-cresol on LNMO, which indicates that the rate-controlling step depends on the number of active sites of the LNMO. On the other hand, the R^2 value of the pseudo-first kinetic model is not satisfactory.

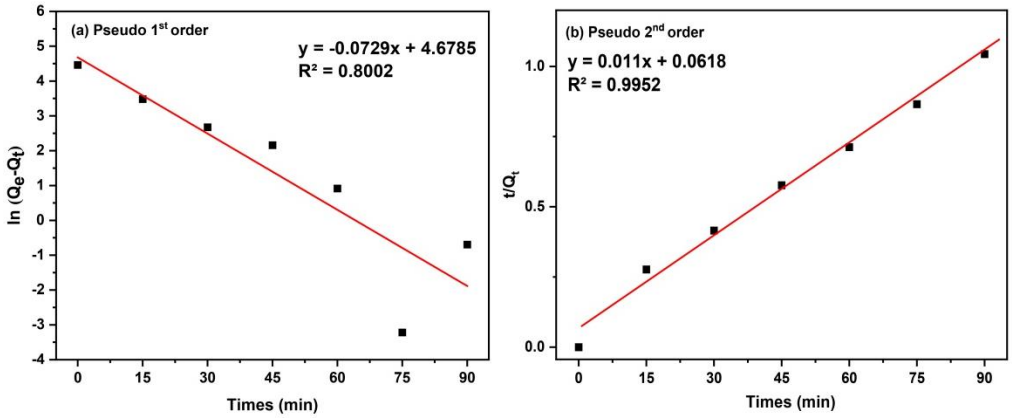

Fig. 5. The adsorption rate of m-cresol on the LNMO double perovskite beads was evaluated using (a) pseudo-first-order and (b) pseudo-second-order kinetic models.

From kinetic analysis, as the pseudo-second order model is well fitted, it can be said that the chemisorption is dominant in the adsorption of m-cresol, which also supports the chemical interactions between the LNMO surface and m-cresol. In addition, the theoretical maximum adsorption capacity of LNMO found from the pseudo-second-order kinetic model is very close to the experimental value.

Table 5 Analysis of pseudo-first order and pseudo-second order kinetic model for the adsorption of m-cresol with LNMO double perovskite

Kinetic Model	Experimental Adsorption Capacity (mg/g^{-1})	Calculated Adsorption Capacity (mg/g^{-1})	Rate Constant (min^{-1})	R^2
Pseudo-first - order	87	46	1.56×10^{-04}	0.800
Pseudo-second- order		91	1.96×10^{-04}	0.995

Investigation of the thermodynamic parameters

The thermodynamic behavior of m-cresol adsorption on LNMO was investigated at different temperatures (298-353 K) using the Van't Hoff equation as depicted in Fig. 6. Moreover, the corresponding values of ΔG^o, ΔH^o, and ΔS^o are summarized in Table 6.

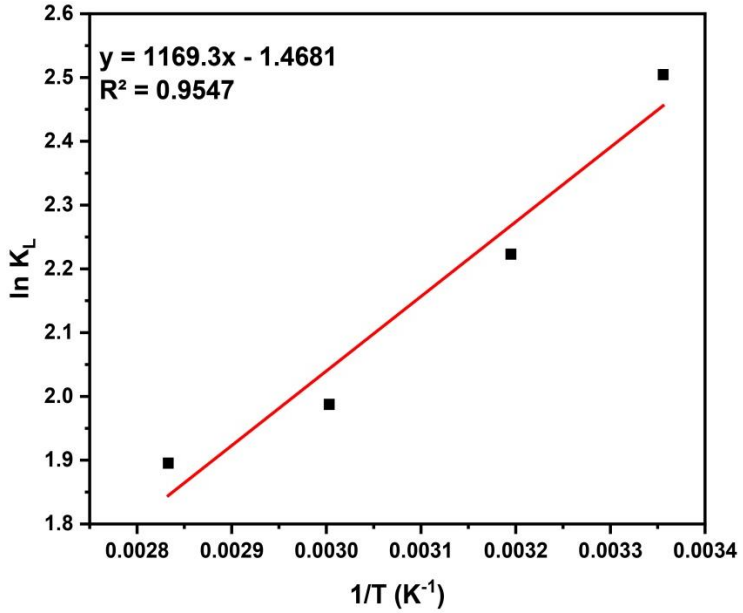

Fig. 6. The Van't Hoff adsorption curve of m-cresol on the LNMO adsorbent.

The negative values of ΔG° across all studied temperatures confirm the spontaneous nature of the adsorption process. Notably, at higher temperature values, the ΔG° becomes less negative, which suggests that, at elevated temperature, the feasibility of adsorption reduces, indicating adsorption is more favorable at lower temperature. The enthalpy change ΔH° was calculated from the slope of the graph; the negative value suggested that the adsorption process mostly follows physisorption. In contrast, kinetic analysis revealed that the adsorption follows a chemisorption mechanism. These findings imply that adsorption on the LNMO surface proceeds through a combination of both physical and chemical interactions. The entropy change ΔS° was found to be -12.11 JK^{-1}, indicating a decrease in randomness at the solid-solution interface during adsorption. Overall, the combined thermodynamic parameters confirm that m-cresol adsorption onto LMNO surface is a spontaneous and entropy-reducing process.

Table 6. Thermodynamic parameters for m-cresol adsorption by LNMO double perovskite

Adsorbent	T (K)	R^2	$\ln K_L$	ΔG^o ($KJmol^{-1}$)	ΔH^o ($KJmol^{-1}$)	ΔS^o ($JK^{-1}mol^{-1}$)
LNMO	298	0.96	2.505	-6.205	-9.72	-12.11
	313		2.223	-5.786		
	333		1.988	-5.503		
	353		1.900	-5.563		

So, this study enlightens that the adsorption of m-cresol onto the LNMO double perovskite nanoparticle is dictated by the operational conditions, especially the pH of the solution. At pH 2, m-cresol remains in its neutral and undissociated form, which promotes the interaction of m-cresol molecules with the LNMO surface. Furthermore, it is evident from the study that LNMO can act as a bifunctional adsorbent due to the presence of Ni^{3+} and Mn^{4+} states,

which may act as an active site for the coordinative binding. Consequently, the adsorption process performed spontaneously, which was confirmed from the analysis of the thermodynamic behavior of the system. The LNMO double perovskite exhibits superior adsorptive capability compared to previously reported adsorbents. This is evident from Table 7, which compares the adsorption capacity of LNMO double perovskite with that of other reported adsorbents.

Table 7. Comparison of phenolic compound adsorption on LNMO double perovskite with different adsorbents

Adsorbent	Phenolic Adsorbate	Isotherm Model	Kinetic model	Maximum Adsorption capacity (mg/g)	Reference
Porous Iron/carbon	m-cresol	Langmuir	Pseudo-second order	120	[35]
ZnO/TiO_2/AC	phenol	Langmuir	Pseudo-second order	95	[36]
Fe_2O_3/mordenite	phenol	Langmuir	Pseudo-second order	95	[37]
Petroleum Asphaltene	m-cresol	Langmuir	Pseudo-second order	127.3	[38]
La_2NiMnO_6 (LNMO)	m-cresol	Langmuir	Pseudo-second order	204	**This work**

IV. Conclusions

This study successfully highlights the potential of LNMO double perovskite nanoparticles as an adsorbent for m-cresol detoxification, demonstrating a simple sol-gel route for their synthesis. The synthesized LNMO material was thoroughly characterized, revealing a hexagonal crystal structure with high phase purity and nanoscale morphology, which positively influenced its adsorption performance. The adsorption of m-cresol was strongly affected by pH, with the best removal efficiency at pH 2. Under these acidic conditions, favorable interactions, including hydrogen bonding and π-π interactions between the aromatic ring of m-Cresol and the metal sites on the LNMO surface, were facilitated. The adsorption kinetics followed a pseudo-second-order model (R^2 = 0.995), indicating that the removal is dominated by a chemisorption process. Additionally, the equilibrium adsorption data were best fitted by the Langmuir isotherm (R^2 = 0.994), suggesting a monolayer adsorption mechanism, with a high maximum adsorption capacity of 204 mg/g^{-1}. Thermodynamic analysis confirmed that the process was both spontaneous and exothermic, indicated by negative values for ΔG^o and ΔH^o. Overall, these findings demonstrate that LNMO double perovskite is a highly effective and promising material for m-cresol removal from wastewater. Its impressive adsorption capacity, favorable thermodynamic properties, and cost-effective synthesis make it an excellent candidate for large-scale applications.

Funding

Bangladesh University of Engineering and Technology, Dhaka, Bangladesh funded the project.

Acknowledgments

The authors acknowledge the lab facilities provided by Nano Chemistry Research Laboratory, Department of Chemistry, Bangladesh University of Engineering and Technology, Dhaka-1000, Bangladesh, for conducting this research work. This work was also supported by Mr. Siraj Mollah, Mr. Md. Hasnat-Uz-Zaman, Mr. Md Nasim Ferdous Kallol, Mr. Md Rashed Nahid Rana, Mr. Md. Shawkat Hossain and Mr. Mohammad Shamsul Islam

Conflicts of Interest

The authors declare no conflict of interest.

References

1. Yang, Y., et al., *Chemical removal of m-cresol: a critical review.* Reviews in Chemical Engineering, 2022. **38**(8): p. 1023-1044.
2. Veeresh, G.S., P. Kumar, and I. Mehrotra, *Treatment of phenol and cresols in upflow anaerobic sludge blanket (UASB) process: a review.* Water research, 2005. **39**(1): p. 154-170.
3. Wang, Y., et al., *Analysis of cardiac developmental toxicity induced by m-cresol in early life of zebrafish and its mechanism.* Comparative Biochemistry and Physiology Part C: Toxicology & Pharmacology, 2025. **289**: p. 110123.
4. Wei, X., et al., *Characterization of phenol and cresol biodegradation by compound-specific stable isotope analysis.* Environmental Pollution, 2016. **210**: p. 166-173.
5. Wang, X. and F. Meng, *Emergency responses to acrylonitrile maritime spills from the perspective of marine ecological protection.* Frontiers in Marine Science, 2022. **9**: p. 996263.
6. Vasileva, E.K., T.I. Parvanova-Mancheva, and V.N. Beschkov, *Classical and new aspects in degradation of aromatic xenobiotics.*
7. Krastanov, A., Z. Alexieva, and H. Yemendzhiev, *Microbial degradation of phenol and phenolic derivatives.* Engineering in Life Sciences, 2013. **13**(1): p. 76-87.
8. Wang, Y., et al., *Mechanistic Insights into m-Cresol Adsorption on Functional Resins: Surface Chemistry and Adsorption Behavior.* Materials, 2025. **18**(15): p. 3628.
9. Said, K.A.M., et al., *A review of technologies for the phenolic compounds recovery and phenol removal from wastewater*. Process Safety and Environmental Protection, 2021. **151**: p. 257-289.
10. Akhtar, M.S., S. Ali, and W. Zaman, *Innovative adsorbents for pollutant removal: exploring the latest research and applications.* Molecules, 2024. **29**(18): p. 4317.

11. Tayari, F., et al., *A comprehensive review of recent advances in perovskite materials: electrical, dielectric, and magnetic properties.* Inorganics, 2025. **13**(3): p. 67.
12. Ibrahim, I., et al., *Water treatment by perovskite materials and their applications: A comprehensive review.* Journal of Industrial and Engineering Chemistry, 2025. **145**: p. 20-32.
13. Deng, C., et al., *Synthesis of poly (ionic liquid) s with high specific surface areas for m-cresol adsorption.* Microporous and Mesoporous Materials, 2023. **362**: p. 112778.
14. Palakkal, J.P., T. Schneider, and L. Alff, *Oxygen defect engineered magnetism of La2NiMnO6 thin films.* AIP Advances, 2022. **12**(3).
15. Deng, H., et al., *Synthesis of fibrous LaFeO3 perovskite oxide for adsorption of Rhodamine B.* Ecotoxicology and Environmental Safety, 2019. **168**: p. 35-44.
16. Shahheydar, A., H. Tavakkoli, and A. Ghaemi, *Fabrication and adsorptive performance of La0. 8Ca0. 2MnO3 perovskite nanoparticles for dye removal process.* Journal of Water Chemistry and Technology, 2022. **44**(6): p. 449-457.
17. Clabel H, J., J. Chacaliaza-Ricaldi, and E. Marega Jr, *Potential application of perovskite structure for water treatment: effects of band gap, band edges, and lifetime of charge carrier for photocatalysis.* Frontiers in Nanotechnology, 2022. **4**: p. 827925.
18. Hossain, A., et al., *An overview of La2NiMnO6 double perovskites: synthesis, structure, properties, and applications.* Journal of Sol-Gel Science and Technology, 2020. **93**(3): p. 479-494.
19. Shinde, K.P., et al., *Electrochemical Investigations of double perovskite M2NiMnO6 (where M= Eu, Gd, Tb) for high-performance oxygen evolution reaction.* Nanomaterials, 2023. **13**(23): p. 3076.
20. Baral, S.C., et al., *Recent advances in La2NiMnO6 double perovskites for various applications; challenges and opportunities.* Progress in Solid State Chemistry, 2023. **72**: p. 100429.
21. Szuromi, P. and B. Grocholski, *Natural and engineered perovskites*. 2017, American Association for the Advancement of Science. p. 732-733.
22. Ali, S.M. and A.A. Eskandrani, *The sorption performance of cetyl trimethyl ammonium bromide-capped La0. 9Sr0. 1FeO3 perovskite for organic pollutants from industrial processes.* Molecules, 2020. **25**(7): p. 1640.
23. Huang, L., et al., *Research progresses on the application of perovskite in adsorption and photocatalytic removal of water pollutants.* Journal of hazardous materials, 2023. **442**: p. 130024.
24. Han, P., et al., *Cation deviated stoichiometry Ca1. 1ZrO3 perovskite as an efficient ozonation catalyst for m-cresol wastewater degradation.* Chemical Engineering Journal, 2022. **429**: p. 132218.
25. D'alessandro, O., H.J. Thomas, and J.E. Sambeth, *An analysis of the first steps of phenol adsorption-oxidation over coprecipitated Mn–Ce catalysts: a DRIFTS study.* Reaction Kinetics, Mechanisms and Catalysis, 2012. **107**(2): p. 295-309.
26. Hossain, M.I., et al., *Synthesis of La2NiMnO6 Double Perovskite as a Highly Selective Electrocatalyst for Oxygen Reduction to Hydrogen Peroxide in Electrochemical Energy Conversion.* ACS Applied Energy Materials, 2025. **8**(2): p. 949-963.
27. Feng, J., et al., *Using activated carbon prepared from Typha orientalis Presl to remove phenol from aqueous solutions.* Ecological Engineering, 2015. **84**: p. 209-217.
28. Dinari, M., R. Soltani, and G. Mohammadnezhad, *Kinetics and thermodynamic study on novel modified–mesoporous silica MCM-41/polymer matrix nanocomposites: effective adsorbents for trace CrVI removal.* Journal of Chemical & Engineering Data, 2017. **62**(8): p. 2316-2329.
29. Yousef, R.I., B. El-Eswed, and H. Ala'a, *Adsorption characteristics of natural zeolites as solid adsorbents for phenol removal from aqueous solutions: kinetics, mechanism, and thermodynamics studies.* Chemical engineering journal, 2011. **171**(3): p. 1143-1149.
30. Islam, M., et al., *Role of strontium as doping agent in LaMn0. 5Ni0. 5O3 for oxygen electro-catalysis.* Journal of Industrial and Engineering Chemistry, 2020. **85**: p. 94-101.
31. Parikh, D., et al., *Structural, Optical, and Dielectric Properties of Double Perovskite La2NiMnO6.* Brazilian Journal of Physics, 2025. **55**(4): p. 175.
32. Zhou, B., et al., *Octahedral distortion and displacement-type ferroelectricity with switchable photovoltaic effect in a 3 d 3-electron perovskite system.* Physical Review Letters, 2023. **130**(14): p. 146101.
33. Han, Y., et al., *Heavy metal and phenol adsorptive properties of biochars from pyrolyzed switchgrass and woody biomass in correlation with surface properties.* Journal of environmental management, 2013. **118**: p. 196-204.
34. Yang, G., et al., *Amination of activated carbon for enhancing phenol adsorption: Effect of nitrogen-containing functional groups.* Applied Surface Science, 2014. **293**: p. 299-305.
35. Bondarenko, G., et al., *m-Cresol Chemisorption on a Porous Iron-Containing Sorbent Prepared from the Carbon Residue after Lignin Processing: I. Pore Structure and Adsorption Ability of the Sorbent.* Petroleum Chemistry, 2021. **61**(1): p. 81-87.
36. Hernández-Barreto, D.F., et al., *Adsorption and photocatalytic study of phenol using composites of activated carbon prepared from onion leaves (allium fistulosum) and metallic oxides (ZnO and TiO_2).* Catalysts, 2020. **10**(5): p. 574.
37. Rashad, A.M., et al., *Removal of phenol using Fe_2O_3/mordenite composite as an efficient adsorbent.* Discover Materials, 2024. **4**(1): p. 81.
38. Ahmed Adam, O.E.-A. and A.H. Al-Dujaili, *The removal of phenol and its derivatives from aqueous solutions by adsorption on petroleum asphaltene.* Journal of Chemistry, 2013. **2013**(1): p. 694029.